Accepted for publication in *Medical Engineering & Physics*

A Complete, Non-Lumped, and Verifiable Set of Upper Body Segment Parameters for Three-Dimensional Dynamic Modeling

Running Head: Upper Body Segment Parameters for 3D Dynamic Modeling

Authors:
Albert H. Vette[1,2], Takashi Yoshida[1,2], T. Adam Thrasher[3], Kei Masani[2], and Milos R. Popovic[1,2]

Affiliations:
[1] Institute of Biomaterials and Biomedical Engineering, University of Toronto,
164 College Street, Toronto, Ontario, M5S 3G9, Canada

[2] Lyndhurst Centre, Toronto Rehabilitation Institute,
520 Sutherland Drive, Toronto, Ontario, M4G 3V9, Canada

[3] Center for Neuromotor and Biomechanics Research, University of Houston,
2450 Holcombe Boulevard, Houston, Texas 77021-2040, USA

September 21, 2010

Corresponding Author:
Albert H. Vette, Dipl.-Ing.
Rehabilitation Engineering Laboratory, Lyndhurst Centre
Toronto Rehabilitation Institute
520 Sutherland Drive, Toronto, Ontario, M4G 3V9, Canada
Phone: +1-416-964-7145 / Fax: +1-416-425-9923
Email: a.vette@utoronto.ca
www.toronto-fes.ca

ABSTRACT

Dynamic models of the human trunk have been extensively used to investigate the biomechanics of lower back pain and postural instability in different populations. Despite their diverse applications, previous models rely on intrinsic upper body segment parameters (UBSP), e.g., each segment's mass-inertia characteristics. However, a comprehensive UBSP set allowing state-of-the-art, three-dimensional (3D) dynamic modeling does not exist to date. Therefore, our objective was to establish a UBSP set of all vertebral trunk segments that is accurate and complete. Based on high-resolution, transverse color images, anatomical structures of the Male Visible Human (MVH) were digitally reconstructed via commercial software. Subsequently, we identified the 3D spinal joint and 3D center of mass coordinates, the mass, and the moment of inertia tensor for 24 vertebral trunk segments and 4 upper limb segments (two segments per arm). Since the MVH images are public domain, the parameters are uniquely verifiable and expandable to also include lower limb parameters. To demonstrate the UBSP set's practicality, the parameters were finally implemented in a previously proposed inverse dynamics model of the upper body. Our findings reveal that an accurate and complete UBSP set has been obtained that will be beneficial to: (1) systemize thinking in postural control studies; (2) quantify the effect of impact forces on the head and trunk (e.g., during whiplash); (3) suggest population-specific experiments based on theoretical insights into trunk dynamics (e.g., regarding lower back pain); or (4) assess the feasibility of new surgical techniques (e.g., spinal fusion) and neuroprostheses (e.g., after spinal cord injury).

INDEX TERMS – Biomechanics; center of mass; dynamic modeling; mass; moment of inertia; spinal joints; the Visible Human Project; trunk; upper limbs.

1. INTRODUCTION

Trunk instability is a major problem for people with spinal cord injury (SCI): it severely compromises their independence in daily life [1] and frequently leads to secondary health complications such as kyphosis [2,3], pressure sores [4], and respiratory dysfunction [5,6]. In fact, a representative survey revealed that people with quadriplegia and paraplegia prioritize the recovery of trunk stability over the recovery of walking function [7]. Furthermore, trunk stability is a key factor in human balance control and mobility – regardless of the population and task. This can be ascribed to the fact that over half of the body's mass is located above the pelvis [8]; as such, the ability to balance the trunk is critical for maintaining stability of the entire body [9].

In exploring mechanisms that may compromise postural stability, linked-segment models have proven very useful [10]. Interest in mathematical modeling of the *upper body* arose in the context of studies on pilot ejection procedures [11,12] that came to the foreground with the advent of high speed aircrafts [13]. More recently, biomechanical trunk models were employed to study intrinsic spine stability [14-20] or the kinetics of vertebral trunk segments during various movements and tasks (e.g., bending or lifting) [21-29]. Other efforts utilized trunk models to predict spinal or head injuries caused by sudden seat displacements [30-33] or to evaluate the feasibility of controlling seated posture after SCI via functional electrical stimulation [34-36].

In spite of their diverse applications, all linked-segment models commonly rely on intrinsic upper body segment parameters (UBSP). For *three-dimensional (3D) dynamic* modeling, these UBSP consist of the 3D joint coordinates as well as each segment's mass, 3D center of mass (COM) location, and moment of inertia tensor [37-39]. Since even small deviations from the true parameter values can, however, lead to substantial errors in the output measures (joint torques or kinematics) [40,41], a dynamic model of the trunk is only as good as the UBSP defining it [42]. Hence, implementing accurate UBSP is of great importance.

Many studies have quantified select UBSP using different subject matter (i.e., cadaver versus living) and techniques [37,38,43-53]. Applied methods include volumetric, photogrammetric, and mechanical torsion techniques [43-46], but more recently also medical diagnostic technologies such as magnetic resonance imaging (MRI) [37], computer tomography (CT) [38,47], gamma ray scanning [48,49,52,53], and X-ray absorptiometry [50,51]. While a few studies identified UBSP for some of the vertebral trunk segments [38,45,46,53], most of the studies reported UBSP for *lumped* trunk portions such as 'upper trunk' and 'lower trunk' [37,43,44,47-52].

All of these efforts offer valuable information for mathematical modeling; none of the studies, however, provide a *complete* set of UBSP that is needed for 3D dynamic modeling. In fact, complete 3 × 3 inertia tensors of the upper body segments and complete 3D coordinates of the underlying joints cannot be found in the literature [37,38,43-53]. Moreover, some reports did not include the location of the segment COM [43,50,53] or reported it in only one dimension [37,49,51]. These shortcomings may be due to the fact that previous studies may not have been driven by 3D dynamic modeling (e.g., [47,50,53]), or that the applied methodology did not allow for identifying such a comprehensive set of 3D parameters (e.g., [45,46]). Besides, only the ever-increasing computer power of recent years has made the implementation and simulation of more realistic and complex 3D models possible [54]. In any case, researchers are still bound to implement UBSP from multiple sources (e.g., [34,35]) and following pre-defined body segmentations (e.g., [8,37,49]), which could potentially compromise the significance of their studies.

To resolve these limitations, the objective of this study was to use publicly available, high-resolution transverse photographs from the *Visible Human Project* [55] to identify a comprehensive set of UBSP for 3D dynamic modeling of the upper body. Particular requirements were that the obtained parameters are: (1) accurate and complete; (2) specified for each vertebral level independently; and (3) entirely verifiable and expandable for complete body modeling. To demonstrate the practicality of the UBSP, they were finally implemented in a complex 3D dynamic model of the upper body to predict spinal joint torques during perturbed sitting (inverse dynamics). The use of such models will be beneficial to: (1) systemize thinking in postural control studies; (2) quantify the effect of impact forces on the head and trunk (e.g., during whiplash); (3) suggest population-specific experiments based on theoretical insights into trunk dynamics (e.g., regarding lower back pain); or (4) assess the feasibility of new surgical techniques (e.g., spinal fusion) and neuroprostheses (e.g., after spinal cord injury).

2. MATERIALS AND METHODS

2.1. Image Properties and Segment Definition

The Visible Human Project was initiated by the *National Institutes of Health* (NIH, USA) in 1988 [55]. Five years later, the Male Visible Human (MVH) was obtained from the body of a 38 year old white male [55]. Having a height of 1.80 m and a weight of 90 kg [55], the subject was centered between the 50th and 75th height and weight percentiles of the general male population [56]. As such, also the overall anthropometrics of the subject should not significantly differ from the average anthropometrics of the general male population [8].

After the frozen body was sectioned with a cryomacrotome at 1 mm intervals, the resulting 1871 transverse body slices were photographed [55,57] with a 70-mm film and digitized at a resolution of 4096 × 2700 pixels [57,58]. Due to this pixilation and the 1-mm spacing of the body slices, each voxel has the size of 0.144 × 0.144 × 1 mm^3 [58]. The 24-bit RGB images (8 bits for Red, 8 bits for Green, and 8 bits for Blue colors) were obtained from the National Library of Medicine and converted to high-resolution JPEG (Joint Photographic Experts Group) images for convenient processing.

Using the JPEG images, a complete set of UBSP was identified for 24 vertebral trunk segments and 4 upper limb segments (two segments per arm). In particular, the trunk was divided into five lumbar segments (L1 to L5), twelve thoracic segments (T1 to T12), six cervical segments (C2 to C7), and the head portion adjacent to the C2 segment (HD)[1]. Note that cervical and head segment parameters are needed for studying whiplash [31-33] as well as the coordination and control of head-trunk dynamics during external perturbations [60-62]. The upper limbs were divided into upper arm segments and forearm-hand segments.

[1] Based on the kinematic analysis of the upper cervical spine by White and Panjabi [59], the neck portion defined by the first cervical vertebra (C1 segment) was included in the head segment HD.

2.2. UBSP Identification

2.2.1. Images Pre-Processing and Reference Frame Definition

949 images from the vertex to the most distal point of the ischium (94.9 cm in height) were pre-processed using a commercial 3D reconstruction software (3D-Doctor, Able Software Corporation, USA). First, anatomical structures were sharpened and their edges enhanced using a high-pass filter whose pixel radius and opacity were based on the image features. To obtain a set of planes that is geometrically accurate, the sharpened images were then realigned across the entire stack. Specifically, neighboring planes were oriented to each other by applying a maximum likelihood algorithm to a central alignment region of 10 × 10 cm^2 that featured strong contrasts, visible patterns, and large variations[2]. These features were ensured by choosing a cross-section of a large number of different anatomical structures.

To dissociate the MVH images from the external reference frame of the digitized photographs $\{F_{VH}\}$ (Fig. 1), a world reference frame $\{F_{WD}\}$ internal to the MVH anatomy was established. As shown in Fig. 1, $\{F_{WD}\}$ was fixed to the right anterior superior iliac spine (ASIS) of the MVH and oriented as to approximate the 'natural' axes of the human body [63]: The Y-coordinate (Y_{WD}) pointed medially from the right to the left ASIS; the X-axis (X_{WD}) was perpendicular to the plane defined by the two ASIS and the midpoint between the pubic tubercles (pointing anteriorly); and the Z-coordinate (Z_{WD}) was the common perpendicular to the first two axes (pointing superiorly) [63]. These conventions resulted in a translation vector ${}^{WD}P_{VHorg}$ and a rotation matrix ${}^{WD}_{VH}ROT$ that transformed any given point from {VH} to {WD}:

[2] The neck and head images demanded smaller alignment regions to avoid including pixels outside the body shell boundary.

$$\begin{bmatrix} {}^{WD}P_x \\ {}^{WD}P_y \\ {}^{WD}P_z \\ 1 \end{bmatrix} = {}^{WD}_{VH}T \begin{bmatrix} {}^{VH}P_x \\ {}^{VH}P_y \\ {}^{VH}P_z \\ 1 \end{bmatrix} = \begin{bmatrix} {}^{WD}_{VH}ROT & {}^{WD}P_{VHorg} \\ 0 \;\; 0 \;\; 0 & 1 \end{bmatrix} \begin{bmatrix} {}^{VH}P_x \\ {}^{VH}P_y \\ {}^{VH}P_z \\ 1 \end{bmatrix} = \begin{bmatrix} 0.056 & 0.998 & 0.028 & -240.558 \\ 0.998 & -0.056 & -0.034 & -146.654 \\ -0.032 & 0.030 & -0.999 & 811.980 \\ 0 & 0 & 0 & 1 \end{bmatrix} \begin{bmatrix} {}^{VH}P_x \\ {}^{VH}P_y \\ {}^{VH}P_z \\ 1 \end{bmatrix} \quad (1)$$

2.2.2. Spinal Joint Centers

In order to identify the spinal joint centers, 3D geometric models were obtained for all spinal discs between the first cervical (C1) and the first sacral vertebrae (S1). Using 3D-Doctor, we traced the disc boundaries on the MVH images and stacked them for geometric volume reconstruction. Since the resulting 3D disc models did not show any undesired artifacts such as protruding edges, only a low level of smoothing was applied to the 3D models that increased the number of face triangles by 20 % (smoothing factor of 0.2 in 3D-Doctor). The obtained models were then used to calculate the 3D COM of each spinal disc, which was assumed to represent the joint about which neighboring vertebral trunk segments could articulate.

The anterior-posterior COM coordinate (AP_{COM}) of a given spinal disc was identified by evaluating the mass-weighted COM coordinates of all 1-mm disc slices via

$${}^{VH}AP_{COM} \cdot m_{Disc} = \sum_{i=1}^{N} {}^{VH}AP_i \cdot m_i \, , \quad (2)$$

where m_{Disc} is the mass of the disc, N the number of the disc's transverse images, ${}^{VH}AP_i$ the AP COM coordinate of the i-th disc slice in {VH}, and m_i the mass of the i-th disc slice. As we assume that the density of each spinal disc is uniformly distributed, Equation (2) can be written as

$${}^{VH}AP_{COM} \cdot \sum_{i=1}^{N} \Delta h \cdot A_i = \sum_{i=1}^{N} {}^{VH}AP_i \cdot \Delta h \cdot A_i$$

$$\Leftrightarrow \quad {}^{VH}AP_{COM} = \frac{\sum_{i=1}^{N} {}^{VH}AP_i \cdot A_i}{\sum_{i=1}^{N} A_i}, \tag{3}$$

where Δh = 1 mm is the thickness of the disc slices and A_i the transverse area of the i-th disc slice. While Equation (3) was also used to identify the superior-inferior coordinate of each spinal disc's COM, the medial-lateral (ML) COM coordinate was assumed to lie in the body's sagittal plane. This plane was perpendicular to Y_{WD} and passed through the midpoint between the pubic tubercles (Fig. 1). Lastly, the obtained 3D coordinates were transformed into {WD}. To verify the validity of the tracing procedure, three spinal discs (C3-C4, T3-T4, and L3-L4) were traced and stacked by an additional researcher. The resulting volume and COM coordinates had an average discrepancy of 0.07 ± 0.06 % with respect to the values identified by the main researcher.

2.2.3. Mass and COM of Vertebral Trunk Segments

The MVH images were also used to create 3D geometric models of the vertebral trunk segments. First, a volumetric representation of the MVH was obtained by tracing and stacking the body shell boundaries of all transverse images in 3D-Doctor. Following, the smoothed body shell model (smoothing factor of 0.2) was divided into vertebral trunk segments using transverse planes that intersected with the COM of the spinal discs [38].

Since the density of the trunk varies substantially along its length [64], the mass of the thoracic and lumbar segments (T1 to L5) was identified via a continuous trunk density function [64]. The densities of the remaining segments (HD and C2 to C7), which were assumed to be uniformly distributed within each segment, were taken from Winter [8]. Accordingly, the mass of a given vertebral trunk segment ($m_{Segment}$) was calculated as

$$m_{Segment} = \delta_{Segment} \cdot V_{Segment} = \sum_{i=1}^{N} \delta_i \cdot \Delta h \cdot A_i \ , \tag{4}$$

where N is the number of the segment's transverse images, Δh = 1 mm the thickness of the segment slices, δ_i the density, and A_i the transverse area of the i-th segment slice.

The AP COM coordinate (AP_{COM}) of a given vertebral trunk segment was again found by evaluating the mass-weighted COM coordinates of each 1-mm segment slice:

$${}^{VH}AP_{COM} \cdot m_{Segment} = \sum_{i=1}^{N} {}^{VH}AP_i \cdot m_i \ , \tag{5}$$

where ${}^{VH}AP_i$ is the AP COM coordinate of the i-th segment slice in {VH}, and m_i the mass of the i-th segment slice. Utilizing the continuous density variation of the trunk along its length [64], Equation (5) yields

$$\begin{aligned} {}^{VH}AP_{COM} \cdot \sum_{i=1}^{N} \delta_i \cdot \Delta h \cdot A_i &= \sum_{i=1}^{N} {}^{VH}AP_i \cdot \delta_i \cdot \Delta h \cdot A_i \\ \Leftrightarrow \quad {}^{VH}AP_{COM} &= \frac{\sum_{i=1}^{N} {}^{VH}AP_i \cdot \delta_i \cdot A_i}{\sum_{i=1}^{N} \delta_i \cdot A_i} \ . \end{aligned} \tag{6}$$

While Equation (6) was also used to identify the superior-inferior COM coordinate of each segment, the ML COM coordinate was again assumed to lie in the body's sagittal plane. Lastly, the obtained 3D coordinates were transformed into {WD}. To verify the validity of the tracing procedure, three trunk segments (C3, T3, and L3) were traced and stacked by an additional researcher. The resulting volume and COM coordinates had an average discrepancy of 0.11 ± 0.08 % with respect to the values identified by the main researcher.

2.2.4. Moment of Inertia of Vertebral Trunk Segments

In order to accurately identify the moment of inertia tensor for each vertebral trunk segment about its COM, the total volume of each segment was dissolved into cubic sub-volumes of V_S = 1 mm^3. This was done by applying Jordan's curve theorem to the polygons of the trunk segment boundaries, i.e., by determining the cube centers that lie within the boundaries of each segment. Taking the continuous density variation of the trunk along its length into account [64], the mass of each cube was then approximated by a point mass ranging between 0.77 and 1.11 mg [8,64]. Using these point masses and their spatial distribution, the principal moments of inertia and products of inertia were calculated as

$$\begin{cases} {}^{VH}_{Jt}I_{xx} = V_S \sum_{i=1}^{N} \delta_i \,(y_i^2 + z_i^2) \\ {}^{VH}_{Jt}I_{yy} = V_S \sum_{i=1}^{N} \delta_i \,(x_i^2 + z_i^2) \\ {}^{VH}_{Jt}I_{zz} = V_S \sum_{i=1}^{N} \delta_i \,(x_i^2 + y_i^2) \end{cases}$$

$$\begin{cases} {}^{VH}_{Jt}I_{xy} = {}^{VH}_{Jt}I_{yx} = -V_S \sum_{i=1}^{N} \delta_i \, x_i \, y_i \\ {}^{VH}_{Jt}I_{xz} = {}^{VH}_{Jt}I_{zx} = -V_S \sum_{i=1}^{N} \delta_i \, x_i \, z_i \\ {}^{VH}_{Jt}I_{yz} = {}^{VH}_{Jt}I_{zy} = -V_S \sum_{i=1}^{N} \delta_i \, y_i \, z_i \end{cases} \tag{7}$$

In Equation (7), x_i, y_i, and z_i identify the location of a particular point mass in {VH} with respect to the segment's COM. The moment of inertia tensors of the vertebral trunk segments were finally transformed from {VH} to {WD} using

$${}^{WD}_{Jt}I_{Segment} = {}^{WD}_{VH}ROT \cdot {}^{VH}_{Jt}I_{Segment} \cdot {}^{WD}_{VH}ROT^{T} \tag{8}$$

2.2.5. Segment Parameters for Upper Limbs

Upper limb parameters were identified for the upper arm (UA) and the forearm-hand segments (FA-H). The upper arm was defined as the portion between the glenohumeral joint center (GHJ) and the midpoint between the humeroulnar and humeroradial joint centers (HURJ). While the 3D joint centers of the upper limbs where directly taken from the MVH images, all other parameters (mass, 3D COM location, and moment of inertia tensor) were calculated as for the trunk segments. As only uniform estimates of the upper limb densities exist [8], we decided to assign different density values to different tissues: (1) bone tissue: 1.90 g/cm^3 [65]; (2) muscle tissue: 1.06 g/cm^3 [66]; and (3) adipose tissue: 0.90 g/cm^3 [67]. For all remaining tissues (mostly blood vessels), a value of 1.00 g/cm^3 was assigned based on the density of water.

2.3. Example Application: Inverse Dynamics for Perturbed Sitting

To demonstrate the completeness of the UBSP and their independence from lumped trunk portions, the identified set was implemented in a previously proposed 3D dynamic model of the upper body that focuses on the actions of the lumbar spine [34]. The model consisted of six rigid bodies, representing five lumbar segments (L1 to L5) and the head-arms-thorax (HAT) complex. The lowest moving segment, i.e., the L5 segment, was located above the pelvis, which served as the inertial frame of reference (Fig. 1). The model had three rotational degrees of freedom between the lowest lumbar segment and the pelvis (L5-S1): flexion-extension, lateral bending, and axial rotation. The remaining five joints were modeled as 3 × 5 rotational constraints. A particular constraint's rotation was defined by: (1) the movement of the 'free' L5-S1 joint; and (2) the ratio between the given joint's and the L5-S1 joint's ranges of motion as reported by White and Panjabi [59].

In order to estimate the lumbar joint torques by applying the inverse dynamics method, the kinematics of each model segment had to be described in inertial frames of reference. The frame assignment of the model followed the Standard Denavit-Hartenberg notation [68] as it elegantly describes the kinematic relationship between the joint variables of the model. To obtain the dynamic model of the upper body, we implemented the identified UBSP in a recursive Newton-Euler formulation of the multi-body dynamics [68]. The model was then used in combination with experimental data from a subject with MVH anthropometrics to predict the lumbar joint torques during perturbed sitting [69,70] (Matlab ver. 7.5, Mathworks Inc., USA). In the experiments, the horizontal force had a Gaussian profile (peak of approximately 200 N), was applied just inferior to the axillae (T7 segment), and perturbed the subject diagonally in the anterior-left direction (five trials). The model implementation was finally validated by solving the same inverse dynamics problem using (1) the Lagrangian formulation [68] and (2) a block diagram within a commercial simulation environment (Simulink ver. 7.4 & SimMechanics ver. 3.1, The MathWorks Inc.). Note that both the Newton-Euler and Lagrangian formulations are 'gold standards' in forward and inverse dynamics calculations [68,71-73]. Block diagram simulations on the other hand are easy to execute, allowing the user to quickly alternate between forward and inverse dynamics applications.

3. RESULTS

The complete UBSP set is available on the worldwide web in form of xls-spreadsheets (Excel), MAT-files (Matlab), and txt-files (www.toronto-fes.ca/upper-body-segment-parameters). The webpage also presents some detailed examples of how to combine the UBSP for models with lumped trunk segments.

3.1. 3D Joint Coordinates and Upper Body Segmentation

The 3D coordinates of the MVH joint centers are listed in Table I. The locations of the vertex and the spinal joint centers from HD-C2 to L4-L5 are expressed in {WD} and given with respect to the subjacent joint in order to capture the joint distances as needed in kinematic modeling. The joint centers of L5-S1 and the upper limb joints are expressed in {WD} and given with respect to $\{F_{WD}\}$. Note that all spinal joint centers were assumed to lie in the body's sagittal plane, resulting in zero ML offsets between the joints (y = 0 in Table I).

Fig. 2 depicts the surface reconstructions of the MVH body shell and spine. The joint centers listed in Table I were used to define the vertebral trunk and upper limb segments, for which respective mass-inertia characteristics were calculated. Note that the segment border between the upper arm and the forearm-hand complex was rotated with respect to the transverse planes to account for the flexion angle of the forearm (Fig. 2).

3.2. Segment Masses, COM Coordinates, and Moment of Inertia Tensors

The utilized segment densities as well as the calculated masses and COM coordinates of all upper body segments are listed in Table II. The COM coordinates of the vertebral trunk segments are expressed in {WD} and given with respect to the subjacent spinal joint center; the COM coordinates of the upper limb segments are expressed in {WD} and given with respect to $\{F_{WD}\}$.

Note that all COM of the vertebral trunk segments were again assumed to lie in the body's sagittal plane (y = 0 in Table II).

Fig. 3 depicts the distribution of the cubic sub-volumes that were used to calculate the moment of inertia tensor for each upper body segment. Note that the sub-volumes are represented by 1-point dots that are positioned at every cube center. Table III shows each segment's principal moments of inertia and products of inertia about the COM with respect to the axes of the world reference frame $\{F_{WD}\}$ (*see Fig. 1*).

3.3. Lumbar Joint Torques during Perturbed Sitting

Fig. 4 depicts the inverse dynamics results for perturbed sitting. Shown are the average perturbation force, the average HAT angles (AP and ML), and the calculated joint torques (AP and ML) for an anterior-left diagonal perturbation. The output torques from the three different inverse dynamics methods are plotted on top of each other. The dashed gray lines in the torque plots mark the predictions for the highest joint (HAT-L1), whereas the dashed black lines mark the predictions for the lowest joint (L5-S1). The torques at the four joints in-between (L1-L2 to L4-L5) are marked by thin and solid gray lines. The vertical line across the subplots indicates the onset of the perturbation force.

A simple visual inspection of Fig. 4 suggests that the joint torque estimations for the three different inverse dynamics formulations coincide. As this observation was supported by an R^2 of over 99.9999 % for different time intervals, the internal validity of the inverse dynamics routines is confirmed. Fig. 4 finally reveals that the AP torque traces are clearly affected by the AP curvature of the spine.

4. DISCUSSION AND CONCLUSIONS

The present paper takes advantage of the Visible Human Project to identify a complete set of upper body segment parameters as needed for state-of-the-art, 3D dynamic modeling. The created UBSP set is particularly useful as its parameters are: (1) accurate and complete; (2) specified for each vertebral level independently; and (3) entirely verifiable and expandable for complete body modeling. In what follows, we elaborate on these advantages in comparison to previously reported UBSP and discuss the implications of the inverse dynamics example.

4.1. Characteristics of UBSP Set

Due to the availability of high-resolution color photographs of the MVH, we could obtain highly accurate 3D surface models of the body shell and spine. The voxels on which the 3D surface reconstructions were based had a size of $0.144 \times 0.144 \times 1$ mm^3 [58]. This resolution, which is significantly higher than in previous reports [37,38,43,44,47,50,51,53], allowed us to minimize errors in boundary tracing and to acquire an accurate stack along the longitudinal body axis. Since all identified UBSP are based on the 3D surface models, the models' quality was essential for identifying *accurate* parameters for the MVH. In addition, the present study obtained a *complete* set of UBSP (3D joint coordinates, segment mass, 3D COM location, and moment of inertia tensor) as needed for 3D dynamic modeling.

One of the main objectives of the present study was to obtain a *flexible* set of parameters that is independent of any pre-defined body segmentations. This goal was accomplished by identifying the parameters for all 24 vertebral trunk segments (HD to L5) and 4 upper limb segments. Since the acquired parameters can be easily combined for different model segmentations (*see www.toronto-fes.ca/upper-body-segment-parameters for detailed procedure*), they should become an important resource for researchers in different fields. For example, in our inverse dynamics application (*see Section 2.3.*), we used the obtained parameters in a model that features five lumbar and a HAT segment [34]. Additional models for which the UBSP set could be harvested have been used to study spinal loads during various tasks [22,24,25,27], whiplash injuries [31-33], and the coordination of head-trunk dynamics [60,62].

Another advantage of the obtained dataset is its verifiability: Since the UBSP were derived from a public domain resource (NIH, USA), other researchers can *verify* our parameters using the outlined identification procedure. Note that this property is unique as the data used in other UBSP reports (e.g., CT [38,47], MRI [37], or cadaver data [45,46]) are study-specific and generally inaccessible to the scientific community. Moreover, the public domain MVH images allow researchers to *expand* the UBSP set to include respective parameters of the lower body.

4.2. Comparison with Previous Studies on UBSP

Also other studies identified select inertial parameters of vertebral trunk segments: Liu and Wickstrom used seven segmented cadavers to identify the masses and AP COM coordinates of the segments as well as their principal moments of inertia [46]. In a study by Pearsall *et al.* [38], CT images of four adults were used to obtain the same parameters. For both studies, the vertebral trunk segment masses and AP COM coordinates exhibited the same profiles along the length of the trunk as in the present study. While the masses were a bit larger for the MVH, the AP COM coordinates with respect to the segments' joints were mostly centered between those reported in [38] and [46]. Finally, the principal moments of inertia were slightly larger in the present study and had a dissimilar profile for the thoracic segments T1 to T4. While the differences in mass and inertia size can be partially explained by differences in subject height and weight, the dissimilar profiles of the thoracic moments of inertia may result from different segmentation boundaries at the glenohumeral joint.

In this context, it has to be emphasized that the discussed studies did not identify complete 3D spinal joint coordinates, 3D COM coordinates, and 3×3 moment of inertia tensors

[38,46]. Moreover, parameters were calculated for the thoracic and lumbar trunk segments (T1 to L5), but not for the cervical trunk or upper limb segments [38,46]. Finally, the obtained parameters in [38] were based on a voxel size of $0.16 \times 0.16 \times 1\ cm^3$, resulting in an overall resolution that was more than 1000 times lower than in the present study. Especially the image spacing of 1 cm must at least partially result in erroneous body segmentations that are not always bounded by the actual spinal disc centers; as a result, respective mass-inertia characteristics must be skewed as well. Considering these shortcomings, the present study is the first to report a set of UBSP that is based on highly accurate surface models and at the same time complete with respect to: (1) the upper body segment definitions; and (2) the parameters needed for 3D dynamic modeling.

4.3. Implications of Inverse Dynamics Application

The inverse dynamics application demonstrated that the identified UBSP can be easily implemented in a 3D model with pre-defined body segments. The example also reveals that the AP curvature of the spine has a distinct effect on the AP torques during body (re-)stabilization. In fact, the static upright posture requires lumbar AP torques of different sign (Fig. 4, before 0 seconds) – a property that is dependent on the AP location of joint centers and segment COM. Moreover, the intersecting of the AP torque traces (Fig. 4, around 0.25 seconds) implies that the lower joints do not necessarily carry larger loads, but that the relative magnitudes depend on the actual trunk kinematics. These are important kinetic observations that are masked in trunk models ignoring the spinal curvature [27,34,35].

4.4. Potential Limitations and their Justification

Since the present study was limited to a single cadaver, we did not establish regression equations for estimating parameters for different subject anthropometrics. Although such scaling rules are beneficial, their identification was not our objective. Instead, the MVH database represented the ideal resource for disseminating an accurate, complete, and verifiable UBSP set of all vertebral trunk segments[3]. The main purpose of the UBSP is to use them independent of subject-specific data, i.e., without the objective of gaining insights into a sample's particular characteristics/conditions. Models implementing the UBSP in forward or inverse dynamics methods will rather represent the human 'per se' to address more basic questions. Such studies are beneficial to: (1) systemize thinking in postural control studies that oftentimes require only a single coherent set of UBSP (e.g., characterization of active & passive control mechanisms); (2) quantify the effect of impact forces on the head and trunk (e.g., during whiplash); (3) suggest population-specific experiments based on theoretical insights into trunk dynamics with and without loads (e.g., regarding lower back pain); or (4) assess the feasibility of new surgical techniques (e.g., spinal fusion) and neuroprostheses (e.g., after spinal cord injury). Studies of this nature are especially important in the context of head and trunk dynamics as technical difficulties either preclude experimental measurements of joint torques or make experiments very time consuming, cumbersome, and error prone [41,76].

The densities within each vertebral trunk segment were assumed to be uniformly distributed along two or three anatomical axes. One reason for this choice was that it is difficult to assign appropriate values to complex connective tissue and organs such as the intestines, the lungs, the kidneys, or the liver. While the chosen approximation may affect the accuracy of respective parameters, the utilized density estimates are still more differentiated than in all previous reports on UBSP. This is the case as we used a recently proposed density function that describes the continuously varying density of the trunk along its length [64]. Moreover, Wicke *et*

[3] It should be emphasized that strong evidence exists that there is no gender difference in postural stability [74,75]. Nevertheless, we acknowledge a potential gender effect on the UBSP; therefore, having a UBSP set for the Female Visible Human may be beneficial as well.

al. revealed that mass-inertia estimates of the trunk are most sensitive to the volume function (which is highly accurate for the MVH), but not very sensitive to the density function [77].

In agreement with previous reports on trunk models [34,35,78], ML asymmetries in the spinal joint centers and trunk segment COM were eliminated during the parameter identification. Unlike other anatomical features that have been retained (such as the AP curvature of the spine or products of inertia entries), these attributes are MVH-specific and not representative for larger samples. Actual ML displacements away from the body's sagittal plane had an average value of 1.7 mm (SD: 1.2 mm) for both the spinal joint centers and trunk segment COM. Using the ML width of the body at different joint and COM heights as a benchmark, this resulted in an overall average error of 0.7 % (SD: 0.5 %). Note that the observed displacement of the spinal joint centers can be mostly attributed to the ML curvature of the spine (minor scoliosis), whereas the displacement of the trunk segment COM is also affected by spine-independent ML body asymmetries.

ACKNOWLEDGEMENT

The authors thank Alan Morris, Vivian Sin, and Roger Xu for their assistance in data acquisition and processing. This work was supported by the Canadian Institutes of Health Research (#86427, #94018, and #97953), the Natural Sciences and Engineering Research Council of Canada, the Ontario Rehabilitation Research Advisory Network, the Ontario Ministry of Health and Long-Term Care, the University of Toronto, and the Toronto Rehabilitation Institute.

CONFLICT OF INTEREST STATEMENT

There are no conflicts of interest for the authors of this study.

LIST OF ABBREVIATIONS

$\{F_{VH}\}$	External Reference Frame (internal to digitized MVH photographs)
$\{F_{WD}\}$	World Reference Frame (internal to MVH anatomy)
{VH}	External Reference System
{WD}	World Reference System
3D	Three-Dimensional
AP	Anterior-Posterior
ASIS	Anterior Superior Iliac Spine
COM	Center Of Mass
CT	Computer Tomography
FA-H	Forearm-Hand Segment
GHJ	Glenohumeral Joint Center
HAT	Head-Arms-Thorax
HURJ	Midpoint between the Humeroulnar and Humeroradial Joint Centers
JPEG	Joint Photographic Experts Group
ML	Medial-Lateral
MRI	Magnetic Resonance Imaging
MVH	Male Visible Human
NIH	National Institutes of Health
RGB	Red-Green-Blue
SCI	Spinal Cord Injury
UA	Upper Arm Segment
UBSP	Upper Body Segment Parameters

REFERENCES

[1] Potten YJM, Seelen HAM, Drukker J, Reulens JPH, Drost MR. Postural muscle responses in the spinal cord injured persons during forward reaching. Ergonomics 1999;42:1200-1215.

[2] Bolin I, Bodin P, Kreuter M. Sitting position – posture and performance in C5-C6 tetraplegia. Spinal Cord 2000;38:425-434.

[3] Alm M, Gutierrez E, Hultling C, Saraste H. Clinical evaluation of seating in persons with complete thoracic spinal cord injury. Spinal Cord 2003;41:563-571.

[4] Gutierrez EM, Alm M, Hultling C, Saraste H. Measuring seating pressure, area, and asymmetry in persons with spinal cord injury. European Spine Journal 2004;13:374-379.

[5] Chen R, Kayser B, Yan S, Macklem PT. Twitch transdiaphragmatic pressure depends critically on thoracoabdominal configuration. Journal of Applied Physiology 2000;88:54-60.

[6] Hart N, Laffont I, de La Sota A, Lejaille M, Macadou G, Polkey M, Denys P, Lofaso F. Respiratory effects of combined truncal and abdominal support in patients with spinal cord injury. Archives of Physical Medicine and Rehabilitation 2005;86:1447-1451.

[7] Anderson KD. Targeting recovery: Priorities of the spinal-cord injured population. Journal of Neurotrauma 2004;21(10):1371-1383.

[8] Winter DA. 'Biomechanics and motor control of human movement'. John Wiley & Sons; New Jersey; 2005.

[9] Kang HG, Dingwell JB. A direct comparison of local dynamic stability during unperturbed standing and walking. Experimental Brain Research 2006;172:35–48.

[10] Pearsall DJ, Reid JG. The study of human body segment parameters in biomechanics: an historical review and current status report. Sports Medicine 1994;18:126-140.

[11] Orne D, Liu YK. A mathematical model of spinal response to impact. Journal of Biomechanics 1971;4:49-71.

[12] Liu YK, von Rosenberg DU. The effects of caudocephalad (+Gz) acceleration on the initially curved human spine. Computers in Biology and Medicine 1974;4:85-106.

[13] Latham F. A study in body ballistics: seat ejection. Proceedings of the Royal Society of London 1957;B147(926):121-139.

[14] Panjabi M, Abumi K, Duranceau J, Oxland T. Spinal stability and intersegmental muscle forces. A biomechanical model. Spine 1989;14(2):194-200.

[15] Crisco JJ 3rd, Panjabi MM. The intersegmental and multisegmental muscles of the lumbar spine. A biomechanical model comparing lateral stabilizing potential. Spine 1991;16(7):793-799.

[16] Shirazi-Adl A, Parnianpour M. Nonlinear response analysis of the human ligamentous lumbar spine in compression. On mechanisms affecting the postural stability. Spine 1993;18(1):147-158.

[17] Cholewicki J, McGill SM. Mechanical stability of the in vivo lumbar spine: implications for injury and chronic low back pain. Clinical Biomechanics 1996;11(1):1-15.

[18] Cholewicki J, Juluru K, McGill SM. Intra-abdominal pressure mechanism for stabilizing the lumbar spine. Journal of Biomechanics 1999;32:13-17.

[19] Granata KP, Wilson SE. Trunk posture and spinal stability. Clinical Biomechanics 2001;16(8):650-659.

[20] Kavcic N, Grenier S, McGill SM. Determining the stabilizing role of individual torso muscles during rehabilitation exercises. Spine 2004;29(11):1254-1265.

[21] McGill SM, Norman RW. Effects of an anatomically detailed erector spinae model on L4/L5 disc compression and shear. Journal of Biomechanics 1987;20(6):591-600.

[22] Jäger M, Luttman A, Laurig W. Lumbar load during one-handed bricklaying. International Journal of Industrial Ergonomics 1991;8:261-277.

[23] Bogduk N, Macintosh JE, Pearcy MJ. A universal model of the lumbar back muscles in the upright position. Spine 1992;17(8):897-913.

[24] McGill SM. A myoelectrically based dynamic three-dimensional model to predict loads on lumbar spine tissues during lateral bending. Journal of Biomechanics 1992;25(4):395-414.

[25] Granata KP, Marras WS. An EMG-assisted model of loads on the lumbar spine during asymmetric trunk extensions. Journal of Biomechanics 1993;26(12):1429-1438.

[26] Granata KP, Marras WS. An EMG-assisted model of trunk loading during free-dynamic lifting. Journal of Biomechanics 1995;28(11):1309-1317.

[27] Gagnon D, Lariviere C, Loisel P. Comparative ability of EMG, optimization, and hybrid modelling approaches to predict trunk muscle forces and lumbar spine loading during dynamic sagittal plane lifting. Clinical Biomechanics 2001;16:359-372.

[28] Daggfeldt K, Thorstensson A. The mechanics of back-extensor torque production about the lumbar spine. Journal of Biomechanics 2003;36:815-825.

[29] Sun LW, Lee RYW, Lu W, Luk KDK. Modelling and simulation of the intervertebral movements of the lumbar spine using an inverse kinematic algorithm. Medical and Biological Engineering and Computing 2004;42:740-746.

[30] Firoozbakhsh K, Balakrishnan R. A model for the response of a passenger's spine to sudden displacement of the seat. Mathematical Biosciences 1978;41:175-187.

[31] Schneider K, Zernicke RF, Clark G. Modeling of jaw-head-neck dynamics during whiplash. Journal of Dental Research 1989;68(9):1360-1365.

[32] Garcia T, Ravani B. A biomechanical evaluation of whiplash using a multi-body dynamic model. ASME Journal of Biomechanical Engineering 2003;125:254-265.

[33] Panjabi MM, Pearson AM, Ito S, Ivancic PC, Wang J-L. Cervical spine curvature during simulated whiplash. Clinical Biomechanics 2004;19:1-9.

[34] Wilkenfeld AJ, Audu ML, Triolo RJ. Feasibility of functional electrical stimulation for control of seated posture after spinal cord injury: A simulation study. Journal of Rehabilitation Research & Development 2006;43(2):139-152.

[35] Lambrecht JM, Audu ML, Triolo RJ, Kirsch RF. Musculoskeletal model of trunk and hips for development of seated-posture-control neuroprosthesis. Journal of Rehabilitation Research & Development 2009;46(4):515-528.

[36] Vanoncini M, Holderbaum W, Andrews B. Development and experimental identification of a biomechanical model of the trunk for functional electrical stimulation control in paraplegia. Neuromodulation 2008;11(4):315-324.

[37] Pearsall DJ, Reid JG, Ross R. Inertial properties of the human trunk of males determined from magnetic resonance imaging. Annals of Biomedical Engineering 1994;22:692-706.

[38] Pearsall DJ, Reid JG, Livingston LA. Segmental inertial parameters of the human trunk as determined from computed tomography. Annals of Biomedical Engineering 1996;24:198-210.

[39] Buchanan TS, Lloyd DG, Manal K, Besier TF. Neuromusculoskeletal modeling: Estimation of muscle forces and joint moments and movements from measurements of neural command. Journal of Applied Biomechanics 2004;20:367-395.

[40] Jensen RK. Human morphology: its role in the mechanics of movement. Journal of Biomechanics 1993;26 (Suppl. 1):81-94.

[41] Hansen L, de Zee M, Rasmussen J, Andersen TB, Wong C, Simonsen EB. Anatomy and biomechanics of the back muscles in the lumbar spine with reference to biomechanical modeling. Spine 2006;31(17):1888-1899.

[42] Panjabi MM, Brand RA, White AA. Three-dimensional flexibility and stiffness properties of the human thoracic spine. Journal of Biomechanics 1976;9:185-192.

[43] Jensen RK. Estimation of the biomechanical properties of three body types using a photogrammetric method. Journal of Biomechanics 1978;11:349-358.

[44] Jensen RK. Changes in segment inertia proportions between 4 and 20 years. Journal of Biomechanics 1989;22:529-536.

[45] Liu YK, Laborde JM, Van Buskirk WC. Inertial properties of a segmented cadaver trunk: their implications in acceleration injuries. Aerospace Medicine 1971;42(6):650-657.

[46] Liu YK, Wickstrom JK. Estimation of the inertial property distribution of the human torso from segmented cadaveric data. In: ‘Perspectives in Biomedical Engineering’. Kenedi RM (ed.), University Park Press, Baltimore, 1973, 203-213.

[47] Erdmann WS. Geometric and inertial data of the trunk in adult males. Journal of Biomechanics 1997;30:679-688.

[48] Zatsiorsky V, Seluyanov V. The mass and inertia characteristics of the main segments of the human body. In: ‘Biomechanics VIII-B’. Matsui H, Kobayashi K (eds.), Human Kinetics Publishers, Champaign, 1983, 1152-1159.

[49] Zatsiorsky VM, Seluyanov VN, Chugunova LG. Methods of determining mass-inertial characteristics of human body segments. In: ‘Contemporary problems of biomechanics’. Chernyi GG, Regirer SA (eds.), CRC Press, Boston, 1990, 272-291.

[50] Wicke J, Dumas GA. Estimating segment inertial parameters using fan-beam DEXA. Journal of Applied Biomechanics 2008;24:180-184.

[51] Wicke J, Dumas GA, Costigan PA. A comparison between a new model and current models for estimating trunk segment inertial parameters. Journal of Biomechanics 2009;42:55-60.

[52] de Leva P. Adjustments to Zatsiorsky-Seluyanov’s segment inertia parameters. Journal of Biomechanics 1996;29:1223-1230.

[53] Duval-Beaupère G, Robain G. Visualization on full spine radiographs of the anatomical connections of the centres of the segmental body mass supported by each vertebra and measured in vivo. International Orthopaedics 1987;11:261-269.

[54] Pandy MG. Computer modeling and simulation of human movement. Annual Review of Biomedical Engineering 2001;3:245-273.

[55] Spitzer V, Ackerman MJ, Scherzinger AL, Whitlock D. The Visible Human Male: a technical report. Journal of the American Medical Informatics Association 1996;3:118-130.

[56] http://www.cdc.gov/nchs/nhanes/nh3data.htm, August 6, 2010.

[57] http://www.nlm.nih.gov/research/visible/getting_data.html, March 1, 2010.

[58] Bonacina S, Menegoni F, Masseroli M, Pinciroli F. Visible Human Dataset color image histograms: 3D web juggler. In: 'Proceedings of the International Federation for Medical and Biological Engineering', vol. 6. Medicon and Health Telematics 2004: Health in the Information Society, Xth Mediterranean Conference on Medical and Biological Engineering, July 31 – August 5, 2004.

[59] White AA, Panjabi MM. 'Clinical biomechanics of the spine', Second Edition. Lippincott Williams & Wilkins; Philadelphia; 1990; pp. 46-49 & 85-125.

[60] Fard MA, Ishihara T, Inooka H. Dynamics of the head-neck complex in response to the trunk horizontal vibration: modeling and identification. ASME Journal of Biomechanical Engineering 2003;125:533-539.

[61] Keshner EA. Head-trunk coordination during linear anterior-posterior translations. Journal of Neurophysiology 2003;89:1891-1901.

[62] Nicholas SC, Doxey-Gasway DD, Paloski WH. A link-segment model of upright human posture for analysis of head-trunk coordination. Journal of Vestibular Research 1998;8:187-200.

[63] Jensen RH, Davy DT. An investigation of muscle lines of action about the hip: A centroid line approach versus the straight line approach. Journal of Biomechanics 1975;8:103-110.

[64] Wicke J, Dumas GA, Costigan PA. Trunk density profile estimates from dual X-ray absorptiometry. Journal of Biomechanics 2008;41:861-867.

[65] Cameron JR, Skofronick JG, Grant RM. 'Physics of the body', Second Edition. Madison; Medical Physics Publishing; 1999.

[66] Mendez J, Keys A. Density and composition of mammalian muscle. Metabolism 1960;9:184-188.

[67] Harrington TAM, Thomas EL, Frost G, Modi N, Bell JD. Distribution of adipose tissue in the newborn. Pediatric Research 2004;55:437-441.

[68] Craig J. 'Introduction to robotics – mechanics and control', Second Edition. Addison-Wesley; New York; 1989 (ed. 2004).

[69] Thrasher TA, Sin VW, Masani K, Vette AH, Craven BC, Popovic MR. Responses of the trunk to multidirectional perturbations during unsupported sitting. Journal of Applied Biomechanics, in press.

[70] Masani K, Sin V, Vette AH, Thrasher TA, Kawashima N, Morris A, Preuss R, Popovic MR. Postural reactions of the trunk muscles to multi-directional perturbations in sitting. Clinical Biomechanics 2009;24(2):176-182.

[71] Asada H, Slotine JE. ‘Robot analysis and control’. Wiley; New York; 1986.

[72] Driels MR, Fan UJ, Pathre US. The application of Newton-Euler recursive methods to the derivation of closed form dynamic equations. Journal of Robotic Systems 1988;5(3):229-248.

[73] Hollerbach JM. A recursive Lagrangian formulation of manipulator dynamics and a comparative study of dynamics formulation complexity. IEEE Transactions on Systems, Man, and Cybernetics 1980;10(11):730-736.

[74] Hageman PA, Leibowitz JM, Blanke D. Age and gender effects on postural control measures. Archives of Physical Medicine and Rehabilitation 1995;76:961–965.

[75] Maki BE, Holliday PJ, Fernie GR. Aging and postural control. A comparison of spontaneous- and induced-sway balance tests. Journal of the American Geriatrics Society 1990;38:1-9.

[76] Goel VJ, Weinstein JN. ‘Biomechanics of the spine: clinical and surgical perspective’. CRC Press; Boca Raton, Florida; 1990; pp. 135-136.

[77] Wicke J, Dumas GA. Influence of the volume and density functions within geometric models for estimating trunk inertial parameters. Journal of Applied Biomechanics 2010;26:26-31.

[78] Stokes IAF, Gardner-Morse M. Quantitative anatomy of the lumbar musculature. Journal of Biomechanics 1999;32:311-316.

Table I. MVH joint centers for all spinal and upper limb joints. The 3D coordinates are expressed in {WD} with respect to the subjacent spinal joint center (spinal joints except L5-S1) or with respect to $\{F_{WD}\}$ (L5-S1 and upper limb joints). All spinal joint centers were assumed to lie in the body's sagittal plane.

Joint	x [mm]	y [mm]	z [mm]	Expressed in {WD}, with respect to
Vertex	-5.801	0	172.656	subjacent spinal joint center
HD-C2	0.948	0	20.039	
C2-C3	1.616	0	19.096	
C3-C4	-0.213	0	18.051	
C4-C5	1.552	0	18.067	
C5-C6	4.907	0	17.106	
C6-C7	9.527	0	18.239	
C7-T1	9.803	0	19.289	
T1-T2	9.494	0	21.273	
T2-T3	7.467	0	21.199	
T3-T4	6.810	0	23.195	
T4-T5	4.234	0	23.120	
T5-T6	2.572	0	24.098	
T6-T7	-0.144	0	25.100	
T7-T8	-2.197	0	24.998	
T8-T9	-4.160	0	25.934	
T9-T10	-3.679	0	24.923	
T10-T11	-3.750	0	29.902	
T11-T12	-9.400	0	32.740	
T12-L1	-9.704	0	35.808	
L1-L2	-11.932	0	35.755	
L2-L3	-8.878	0	38.780	
L3-L4	-4.886	0	38.913	
L4-L5	3.249	0	39.054	
L5-S1	-56.683	123.551	40.279	$\{F_{WD}\}$
rGHJ	-89.198	-34.148	488.119	$\{F_{WD}\}$
rHURJ	-117.901	-127.199	200.176	
lGHJ	-80.030	280.416	486.762	
lHURJ	-106.983	356.487	205.168	

Table II. Densities, masses, and COM coordinates for all upper body segments. The COM coordinates are expressed in {WD} with respect to the subjacent spinal joint center (HD to L5) or with respect to $\{F_{WD}\}$ (upper limb segments). All COM of the vertebral trunk segments were assumed to lie in the body's sagittal plane.

Segment	Density [g/cm^3]	Mass [kg]	COM			Expressed in {WD}, with respect to
			x [mm]	y [mm]	z [mm]	
HD	1.11 [8]	3.752	-0.090	0	70.718	
C2	1.11 [8]	0.514	5.380	0	10.257	
C3	1.11 [8]	0.459	3.578	0	9.759	
C4	1.11 [8]	0.434	-3.262	0	8.760	
C5	1.11 [8]	0.532	-20.076	0	7.986	
C6	1.11 [8]	0.696	-29.729	0	7.064	
C7	1.11 [8]	1.029	-23.228	0	7.883	
T1	f(z)={1.00-1.01} [64]	1.247	-14.056	0	8.788	
T2	f(z)={0.97-1.00} [64]	1.584	-2.656	0	10.240	
T3	f(z)={0.92-0.97} [64]	1.410	6.901	0	10.877	
T4	f(z)={0.86-0.92} [64]	1.434	17.616	0	12.153	
T5	f(z)={0.80-0.86} [64]	1.349	27.803	0	12.378	subjacent spinal joint center
T6	f(z)={0.77-0.80} [64]	1.332	35.851	0	13.284	
T7	f(z)={0.77-0.78} [64]	1.533	39.643	0	13.766	
T8	f(z)={0.78-0.81} [64]	1.572	41.575	0	13.697	
T9	f(z)={0.81-0.86} [64]	1.700	39.873	0	14.144	
T10	f(z)={0.86-0.91} [64]	1.694	38.440	0	13.610	
T11	f(z)={0.91-0.96} [64]	2.113	37.827	0	16.046	
T12	f(z)={0.96-1.00} [64]	2.403	33.825	0	17.450	
L1	f(z)={1.00-1.01} [64]	2.621	30.324	0	19.021	
L2	f(z)={0.96-1.00} [64]	2.541	22.478	0	18.844	
L3	f(z)={0.91-0.96} [64]	2.624	13.168	0	20.094	
L4	f(z)={0.89-0.91} [64]	2.520	7.678	0	19.826	
L5	f(z)={0.89-0.93} [64]	2.588	5.982	0	19.380	
rUA	0.90-1.90 [65-67]	3.051	-97.131	-97.277	339.645	
rFA-H	0.90-1.90 [65-67]	1.823	-11.144	-56.979	93.938	$\{F_{WD}\}$
lUA	0.90-1.90 [65-67]	2.998	-87.783	338.120	333.170	
lFA-H	0.90-1.90 [65-67]	1.785	-10.007	300.026	96.554	

Table III. Principal moments of inertia (left) and products of inertia (right) for all upper body segments. The moments of inertia are expressed in {WD} and given for rotations about the segment's COM.

Segment	Principal Moments of Inertia			Products of Inertia		
	I_{XX}	I_{YY}	I_{ZZ}	$I_{XY} = I_{YX}$	$I_{XZ} = I_{ZX}$	$I_{YZ} = I_{ZY}$
	[kg cm^2]					
HD	120.673	155.404	139.038	1.373	1.555	-2.050
C2	7.602	12.315	19.538	0.175	-0.356	0.248
C3	6.295	10.506	16.491	0.051	-0.334	0.198
C4	6.489	9.749	15.959	0.410	-0.367	0.251
C5	16.235	10.774	26.637	0.639	-0.478	0.623
C6	48.401	10.634	58.573	-1.931	-0.274	1.581
C7	114.159	17.631	130.978	-4.045	-0.374	3.643
T1	174.195	25.937	198.975	-5.235	-0.526	5.654
T2	246.231	39.634	284.122	-6.887	-0.781	8.047
T3	187.651	51.707	237.662	-5.244	-1.127	6.178
T4	186.822	67.763	252.498	-6.774	-1.484	6.086
T5	189.944	77.123	264.927	-6.732	-1.711	6.056
T6	195.278	88.820	281.643	-7.388	-2.026	6.358
T7	141.048	72.025	211.093	-5.415	-1.642	4.560
T8	139.368	76.841	214.164	-5.024	-1.872	4.527
T9	143.337	84.103	225.089	-4.417	-2.110	4.700
T10	134.204	83.833	215.857	-4.489	-2.102	4.408
T11	158.157	106.230	260.745	-6.166	-2.503	5.113
T12	169.439	123.855	288.430	-6.813	-2.780	5.487
L1	174.895	136.548	305.256	-6.477	-3.077	5.600
L2	167.440	130.985	292.390	-3.528	-3.375	5.396
L3	182.594	133.226	308.557	-2.436	-3.622	5.939
L4	183.898	125.476	302.358	-0.947	-3.510	6.063
L5	198.149	126.160	317.040	-2.007	-4.018	6.337
rUA	197.754	211.134	48.401	-6.452	-4.581	-12.318
rFA-H	130.280	162.556	117.193	-54.761	71.102	51.912
lUA	158.132	169.848	45.751	5.177	-7.394	6.111
lFA-H	119.798	153.203	96.517	39.119	67.181	-43.011

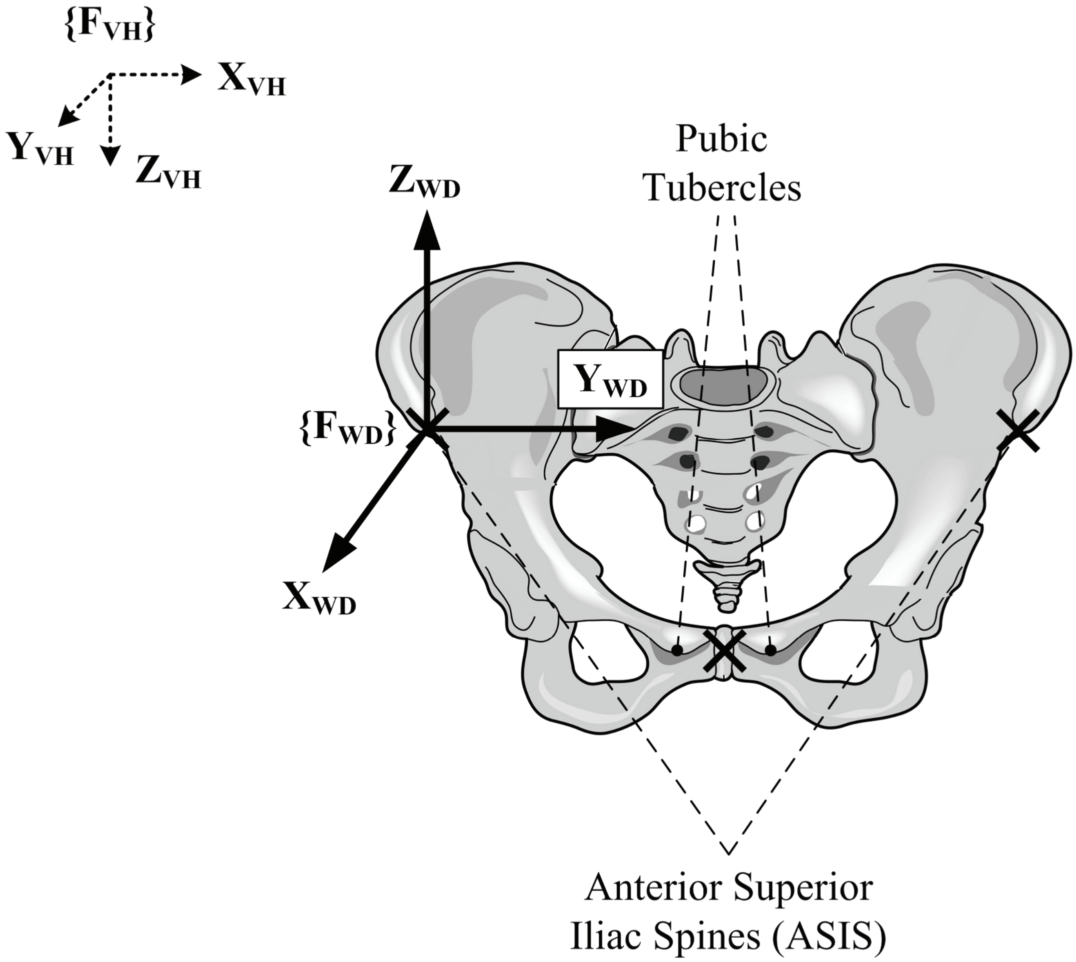

Fig. 1. Anterior view of the pelvis and three bony landmarks that define the world reference frame $\{F_{WD}\}$. The bony landmarks were the right and left anterior superior iliac spines (ASIS) and the midpoint between the pubic tubercles (marked as '×').

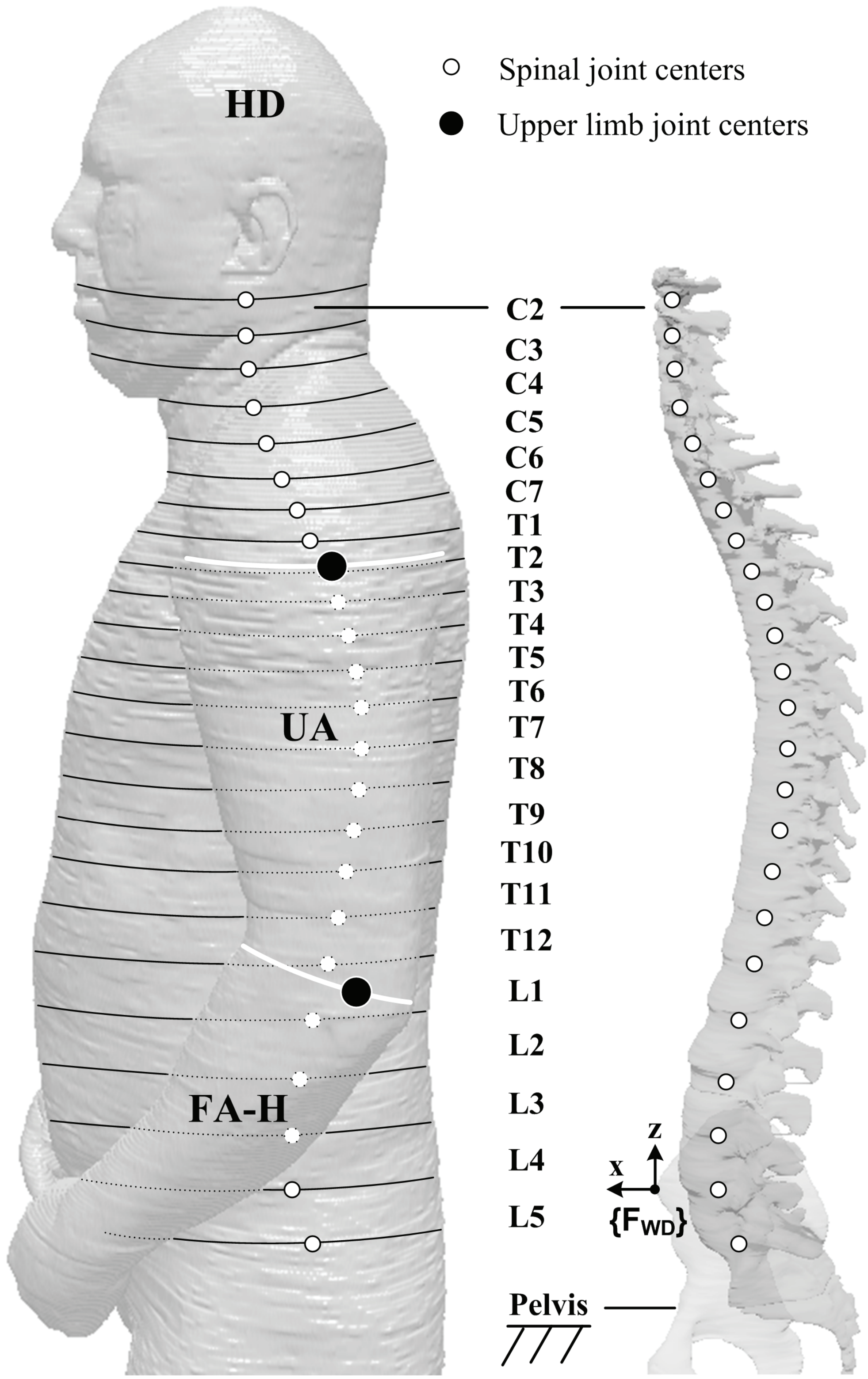

Fig. 2. Surface models of the MVH body shell and spine. The joint centers listed in Table I were used to define the upper body segments for which respective mass-inertia characteristics were calculated.

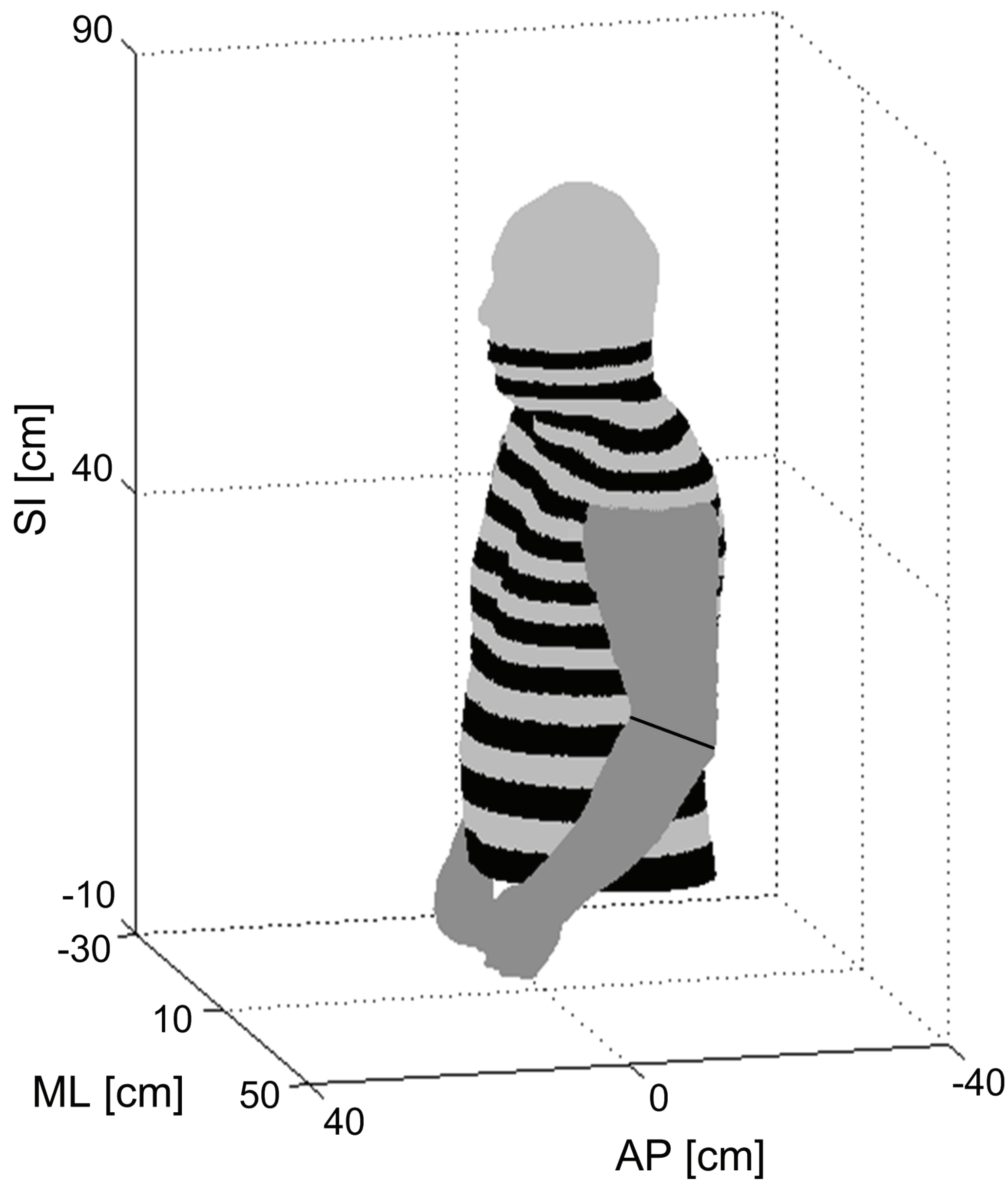

Fig. 3. Distribution of the cubic sub-volumes for all upper body segments. The sub-volumes are represented by 1-point dots that are positioned at every cube center.

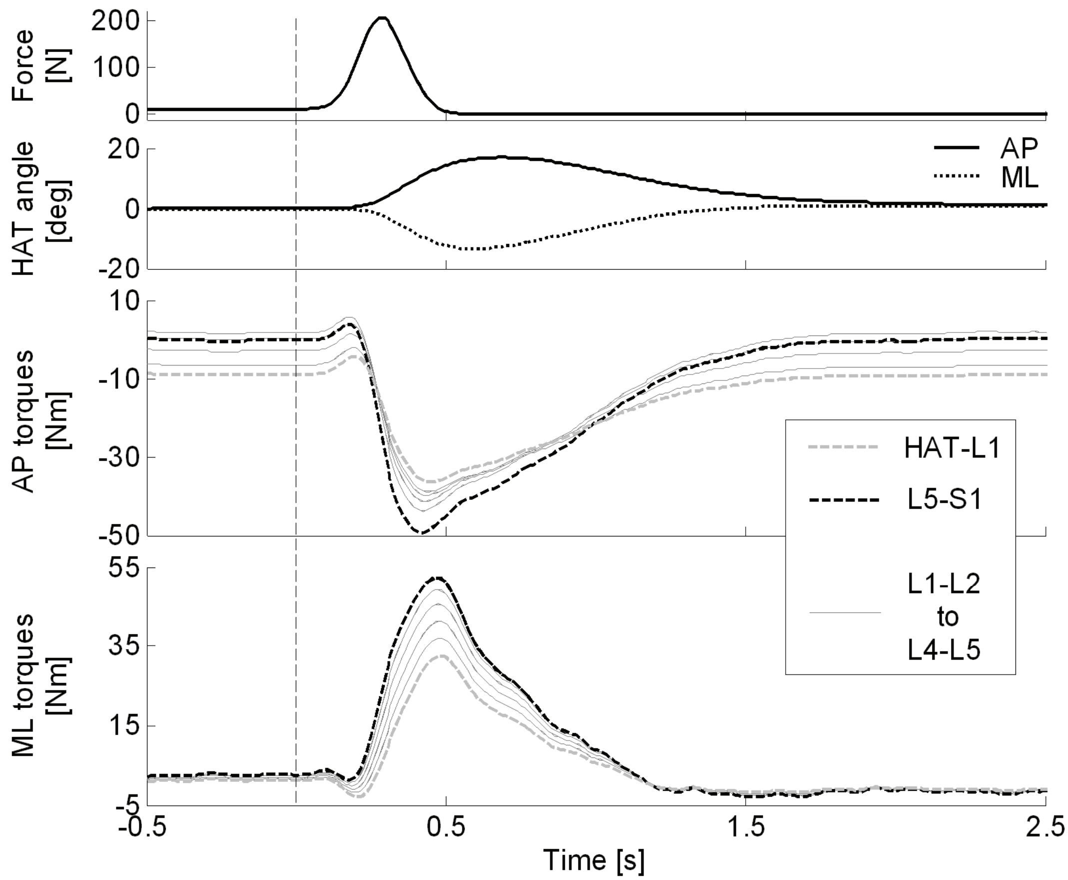

Fig. 4. Inverse dynamics results for perturbed sitting. Shown are the average perturbation force, the average HAT angles (AP and ML), and the calculated joint torques (AP and ML) for an anterior-left diagonal perturbation. The output torques from the three different inverse dynamics methods are plotted on top of each other (not distinguishable). The dashed gray lines in the torque plots mark the predictions for the highest joint (HAT-L1), whereas the dashed black lines mark the predictions for the lowest joint (L5-S1). The torques at the four joints in-between (L1-L2 to L4-L5) are marked by thin and solid gray lines. The vertical line across the subplots indicates the onset of the perturbation force.